A model of the mechanics of the left ventricle

Annals of Biomedical Engineering, Vol. 7, pp. 299-318, 1979
Printed in the USA.
0191-5649/79/030299-20$02.00/0

A MODEL OF THE MECHANICS OF THE LEFT VENTRICLE

Theo Arts

Department of Biophysics

Robert S. Reneman

Department of Physiology
University of Limburg, Maastricht, The Netherlands

and

Peter C. Veenstra

Department of Mechanical Engineering
University of Technology, Eindhoven, The Netherlands

The relation between cardiac muscle mechanics and left ventricular (LV) pump function is simulated by a mathematical model. In the following article special attention is paid to the relation between LV pressure and LV volume on the one hand and the transmural distribution of sarcomere length and fiber stress on the other. The LV is simulated by a thick-walled cylinder composed of 8 concentric shells. The myocardial material is assumed to be anisotropic. The orientation and sequential activation of the muscle fibers across the LV wall are considered per shell. Twisting of the base with respect to the apex around the axis of the LV is simulated by rotation of the upper cross-sectional surface of the cylinder with respect to the lower one around the axis of the cylinder.

The model reveals that twisting of the LV is an important means to equalize transmural differences in sarcomere shortening and end-systolic fiber stress. When torsion is allowed, transmural differences in sarcomere shortening and end-systolic fiber stress are less than 18% and 16%, respectively. When torsion is prevented as in most of the models of LV-mechanics described in literature, these transmural differences increase up to 32% and 42%, respectively.

INTRODUCTION

Several models of the mechanics of the left ventricle have been described in literature. In these models assumptions are made about the shape of this

Supported by the Foundation for Medical Research FUNGO, which is subsidized by the Netherlands organization for the Advancement of Pure Research.

Requests for reprints may be sent to Theo Arts, Department of Biophysics, Biomedical Centre, University of Limburg, P.O. Box 616, 6216 EA Maastricht, The Netherlands.

ventricle. Hanna (8) and Mirsky (16) proposed a sphere as a model for the geometry of the left ventricle. A more accurate description of this geometry is a prolate ellipsoid as proposed by Hood et al. (10), Mirsky (15), Streeter et al. (25) and Wong et al. (29). Janz et al. (12, 13) and Pao et al. (17, 18) applied the finite element method to an experimentally determined, but more complicated geometry of the heart.

When studying the dynamics of the left ventricle, the choice of the geometry of the left ventricle is rather important because the relation between wall stress and left ventricle pressure depends on this geometry. From studies of McHale et al. (14) and Back (3) it can be concluded that the calculated wall stress is approximately 50% less if a spherical rather than an ellipsoidal geometry is assumed.

An additional problem is that the calculated stress distribution across the myocardial wall depends, among other things, on the mechanical properties of the myocardial material as introduced in the model. Many authors (7, 10, 12, 13, 15, 16, 17, 18, 29) assumed isotropy of the myocardial material. The myocardium, however, mainly consists of anisotropic muscle material. Models based on isotropic myocardial material introduce large errors in describing the process of ejection and the transmural distribution of stresses (1, 2). During ejection the simulated, isotropic left ventricle appears to be three times stiffer than the real ventricle in an anesthetized dog. Hence, in models based on isotropy of the cardiac muscle, the mechanics of the heart cannot be described adequately.

The model introduced by Streeter et al. (26) includes ellipsoidal geometry, anisotropy of the myocardial material and changing fiber orientation across the wall. In their model, however, large deformations, which occur during ventricular ejection, could not be described adequately because of the applied mathematics.

Because of the assumption of isotropic myocardial material, the introduction of an inadequate geometry of the left ventricle—a sphere rather than an ellipsoid—not taking into account the fiber orientation in the left ventricular wall or the impossibility to describe large deformations, the models presented up to now in literature are less suitable to study the transmural course of wall stress and the mechanics of left ventricular contraction. Therefore, a new model was developed in which all these factors were considered.

This article describes a mathematical model of the relation between instantaneous values of left ventricular volume, pressure and dimensions as well as the transmural course of stress and sarcomere length in the left ventricle. This model is the basis of a larger model, describing the left ventricular mechanics. The larger model will not be discussed in detail in this article.

PRINCIPLES OF THE MATHEMATICAL MODEL

In designing a mathematical model of the mechanics of the left ventricle, simplifications concerning the characteristics of the heart are required. Each

simplification is a compromise between accuracy and simplicity. In the present model the following simplifications were made:

- Only the left ventricle is simulated.
- The left ventricle is a thick-walled cylinder composed of 8 concentric cylindrical shells (Fig. 1). The most realistic results for the relation between left ventricular pressure and wall stress are obtained if ellipsoidal geometry is assumed. Cylindrical geometry, however, approximates these results closely, i.e., within 10%, and significantly better than if spherical geometry is assumed (1).
- Anisotropy of the myocardial material is introduced by assuming that the myocardial tissue consists of a contractile fiber structure embedded in a soft incompressible material (2).
- The contractile fiber structure is assumed to be a stiff spring. The prelength, defined as the sarcomere length after a quick release to zero load, changes during the cardiac cycle as a function of the degree of activation of the cardiac muscle. The difference between actual sarcomere length and prelength is about 2%, which is based on the results of cardiac muscle obtained in *in vitro* experiments (19).
- The fiberorientation (25) and sarcomere length (11, 30) change across the wall, and the spread of activation was considered to proceed only in radial direction with a velocity of 0.4 m s^{-1} (5, 22). However, within a cylindrical shell all fibers have the same orientation, the same load, the same sarcomere length and a similar degree of activation. Transmural gradients of these quantities are presented as stepwise changes from shell to shell.

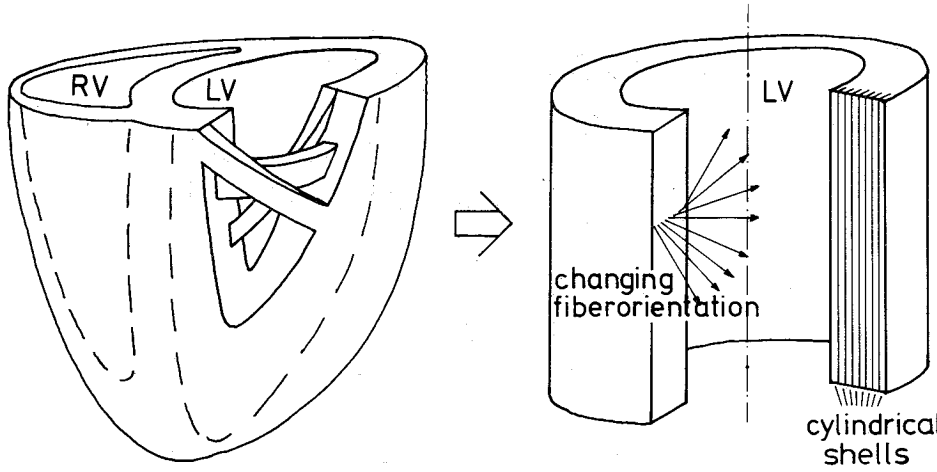

FIGURE 1. Schematic representation of the geometry of the left ventricle. The left ventricle is simulated by a cylinder. Subdivision of the thick-walled cylinder in a number of shells and changing fiber orientation are indicated.

CALCULATION OF THE INSTANTANEOUS STATE OF MECHANICAL LOADING OF THE LEFT VENTRICLE

Calculation Procedure

The quantities related to the stress in the wall of the cylinder, representing the left ventricle, were calculated from the volume of the cavity enclosed by the cylinder, the volume of each cylindrical shell and the instantaneous values of prelength and stiffness of the muscle fiber structure in each shell. The quantities, thus calculated, were dimensions and torsion angle of the cylinder, local stress and sarcomere length, local intramyocardial pressure and left ventricular pressure. The torsion angle α is defined as the angle over which the upper cross-sectional surface of the cylinder is rotated around the axis with respect to its lower cross-sectional surface (Fig. 2). This angle represents the angle of rotation of the base with respect to the apex around the axis of the left ventricle.

A block diagram of the sequence of calculation is shown in Fig. 3. After a first estimate of the height and torsion angle of the cylinder the dimensions and torsion angle of each shell were calculated using the volumes of the cavity and the shells. Subsequently in each shell sarcomere length and fiber stress were calculated by applying the instantaneous values of prelength and stiffness of the myocardial material. Next total axial force and torque, acting on the upper surface of the cylinder including the cavity, were calculated. Conditions of equilibrium require that these equal zero. If either one or both quantities exceed a chosen criterion, new estimates of the height and torsion angle were calculated. Finally if the deviations from the equilibria were sufficiently small, the iteration procedure was stopped and left ventricular pressure and radial stresses were computed.

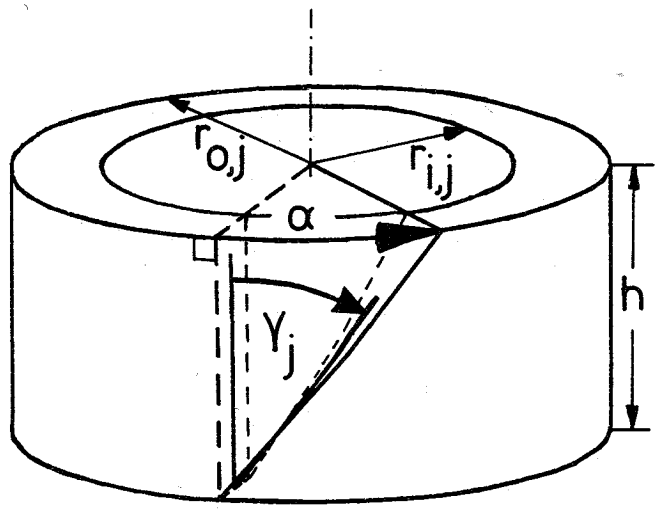

FIGURE 2. The upper surface of a cylindrical shell is rotated over the torsion angle α due to deformation of the shell. The shear angle γ_j, inner radius $r_{i,j}$, outer radius $r_{o,j}$ and height h are indicated.

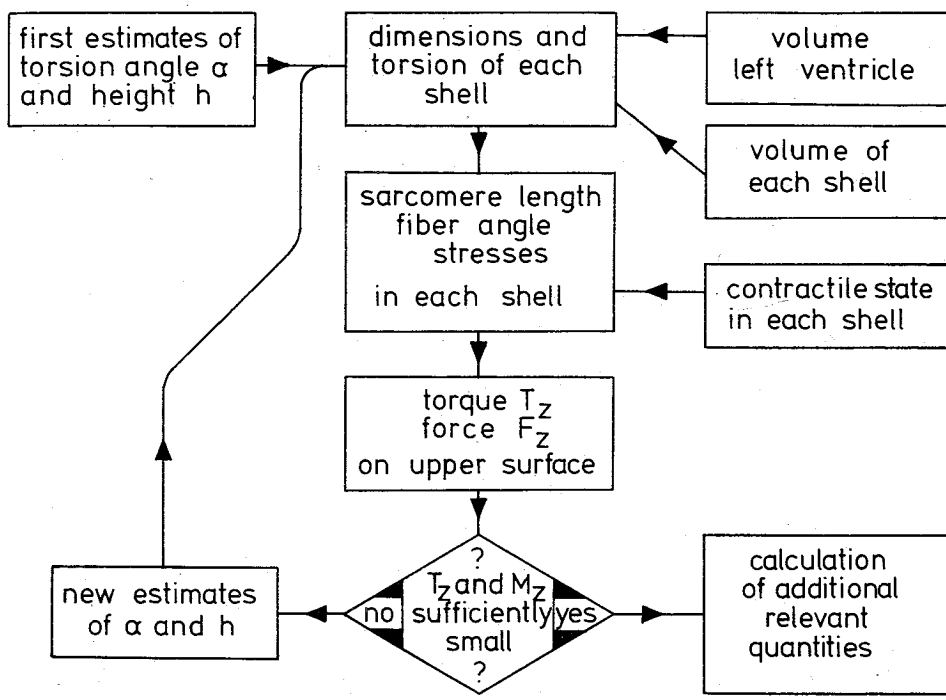

FIGURE 3. Block diagram of the sequence of calculations in order to obtain the state of deformation of the cylinder, which simulates the left ventricle.

Determination of Dimensions and Torsion Angle of Each Cylindrical Shell

The thick-walled cylinder, representing the left ventricle, is composed of n cylindrical shells. The shells are numbered off from the inner one. Generally it holds that

– the cylindrical shells remain in contact with each other, which is expressed by

$$r_{o,j} = r_{i,j+1} \qquad 1 \leqslant j \leqslant n-1 \tag{1}$$

where

$r_{o,j}$ = outer radius of shell j
$r_{i,j+1}$ = inner radius of shell j+1
j = ordinal number of the shell

– the height of all cylindrical shells is the same, thus

$$h_j = h \qquad 1 \leqslant j \leqslant n \tag{2}$$

where

h_j = height of shell j
h = height of the cylinder

– the radial coordinate is assumed to be a principal direction of the strain rate tensor, and hence

$$\alpha_j = \alpha \qquad 1 \leqslant j \leqslant n \tag{3}$$

where

α_j = torsion angle of shell j
α = torsion angle of the cylinder

Applying Eqs. 1 and 2 the dimensions of each shell can be determined from the height h of the cylinder and the volumes of the inner cavity (V_{lv}) and the shells (V_j). The inner radius of the cylinder (r_{iv}) is given by

$$r_{iv} = \sqrt{\frac{V_{lv}}{\pi h}} = r_{i,1} \tag{4}$$

Using Eq. 1 in successive steps, the outer radius of each shell is determined by

$$r_{o,j} = \sqrt{r_{i,j}^2 + \frac{V_j}{\pi h}} \tag{5}$$

It should be noticed that only the estimated values of the height h and torsion angle α are known.

Computation of the Stresses in a Cylindrical Shell

Both the dimensions of a shell and the torsion angle determine the deformation of the wall material. The dimensions of shell j are the height h, the inner radius $r_{i,j}$ and the outer radius $r_{o,j}$. These dimensions and the torsion angle α are shown in Fig. 2. In the initial state the values of these dimensions are denoted as H, $R_{i,j}$ and $R_{o,j}$, respectively, whereas $\alpha = 0$. The average values of the natural strain in the wall are given by

$$\epsilon_{r,j} = \ln \left[\frac{r_{o,j} - r_{i,j}}{R_{o,j} - R_{i,j}} \right] \tag{6}$$

$$\epsilon_{t,j} = \ln \left[\frac{r_{o,j} + r_{i,j}}{R_{o,j} + R_{i,j}} \right] \tag{7}$$

$$\epsilon_{z,j} = \ln \left[\frac{h}{H} \right] \tag{8}$$

where r, t and z respectively are the radial, tangential and axial coordinates. The shear angle γ_j (Fig. 2) which defines the shear deformation in the center plane of the shell is given by

$$\tan \gamma_j = \frac{\alpha(r_{o,j} + r_{i,j})}{2h} \tag{9}$$

For further calculations a rectangular area of the center plane of shell j in the initial state of deformation is considered (Fig. 4). The sides of this rectangle are chosen to be parallel to the tangential and axial coordinates. One diagonal is parallel to the initial fiber direction and the length is equal to the initial sarcomere length $l_{so,j}$. The initial fiber angle, which is defined as the angle between the initial fiber direction and the t-coordinate, is denoted as $\beta_{o,j}$.

After deforming the shell according to Eqs. 6, 7 and 8, the rectangle is distorted to a parallelogram as shown in Fig. 4. For the projections of the diagonal on the t- and z-coordinate, $l_{t,j}$ and $l_{z,j}$ respectively, it holds

$$l_{t,j} = [\tan(\gamma_j) \exp(\epsilon_{z,j}) \sin(\beta_{o,j}) + \exp(\epsilon_{t,j}) \cos(\beta_{o,j})] l_{so,j} \tag{10}$$

$$l_{z,j} = \exp(\epsilon_{z,j}) \sin(\beta_{o,j}) \cdot l_{so,j} \tag{11}$$

The instantaneous sarcomere length is calculated through

$$l_{s,j} = \sqrt{l_{t,j}^2 + l_{z,j}^2} \tag{12}$$

and the instantaneous fiber angle β_j through

$$\beta_j = \arctan \left[\frac{l_{z,j}}{l_{t,j}} \right] \tag{13}$$

The fiberstress $\sigma_{f,j}$ in shell j is calculated from the instantaneous values of sarcomere length $l_{s,j}$, zero load sarcomere length $l_{pr,j}$ and sarcomere stiffness $K_{s,j}$ as

$$\sigma_{f,j} = (l_{s,j} - l_{pr,j}) K_{s,j} \tag{14}$$

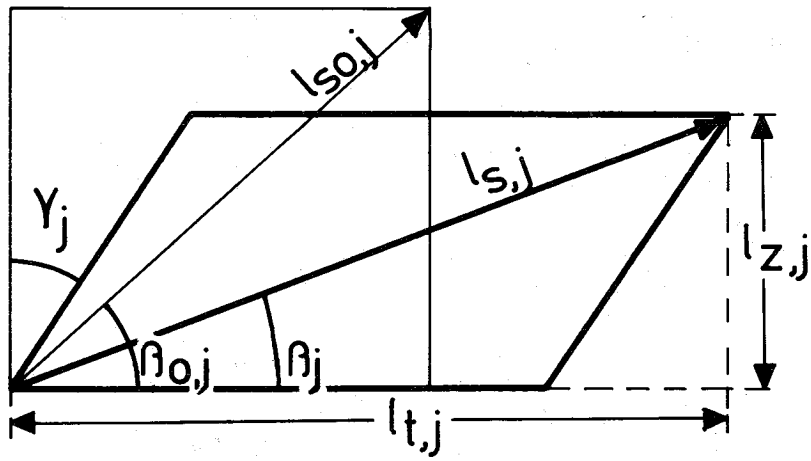

FIGURE 4. Deformation of a rectangular area to a parallelogram in the center plane of a cylindrical shell during contraction.

The quantities $l_{pr,j}$ and $K_{s,j}$ are determined by the degree of activation and contraction of the cardiac muscle in shell j. Their values change with time and are different in each shell. Equation 14 enables substitution of all kinds of mathematical descriptions of the stress-sarcomere length-velocity of sarcomere shortening-time relation. A sample of such a description is the variable elastance model of Sagawa (21) in which the value of the quantity $l_{pr,j}$ is constant (approximately 1.6 μm) and the value of $K_{s,j}$ changes with time.

The stress $\sigma_{f,j}$ acts on the muscle fibers, which make an angle β_j with the cross-sectional plane of the cylindrical shell. Applying general laws of stress to the fiber stress $\sigma_{f,j}$, the normal stress $\sigma_{fz,j}$ in axial direction, the normal stress $\sigma_{ft,j}$ in tangential direction and the shear stress $\sigma_{ftz,j}$ in the upper surface of the shell can be formulated as

$$\sigma_{ft,j} = \sigma_{f,j} \cos^2 \beta_j \tag{15}$$

$$\sigma_{fz,j} = \sigma_{f,j} \sin^2 \beta_j \tag{16}$$

$$\sigma_{ftz,j} = \sigma_{f,j} \cos \beta_j \sin \beta_j \tag{17}$$

According to the concept of anisotropic material, in each shell a hydrostatic component ($-p_{im}$) in the soft material surrounding the myocardial fibers can be added to the normal stresses.

Equilibrium of Force and Torque Acting on the Upper Surface of the Cylinder

For solving the height and torsion angle of the cylinder two equations are necessary. One equation is based on the equilibrium of axial forces acting on the upper surface of the cylinder, and the other is based on the equilibrium of torques acting on this surface around the axis of the cylinder.

The force acting in the axial direction on the upper surface of the cylinder is the sum of the force exerted by the left ventricular pressure acting on the upper surface of the cavity and the force exerted by axial stresses in the different shells. In the model for each shell the contribution $\Delta F_{z,j}$ to the total force F_z acting on the upper surface of the cylinder is calculated from the axial stress acting on the upper surface of that shell and the left ventricular pressure increment as generated by the tangential stress. The latter pressure is assumed to act on the surface, which corresponds to the radius of the center plane of the shell (Fig. 5). Thus it holds

$$\Delta F_{z,j} = \pi(\sigma_{fz,j} - \frac{1}{2}\sigma_{ft,j})(r_{o,j}^2 - r_{i,j}^2) \tag{18}$$

Obviously $\Delta F_{z,j}$ is independent of externally applied hydrostatic pressure, since shells and cavity content are supposed to be incompressible. The conclusion is that $\Delta F_{z,j}$ only depends on the stress in the fiber structure as expressed by Eq. 18. Figure 6 shows schematically the composition of the total axial force acting on the system of shells. Each shell is supposed to be sur-

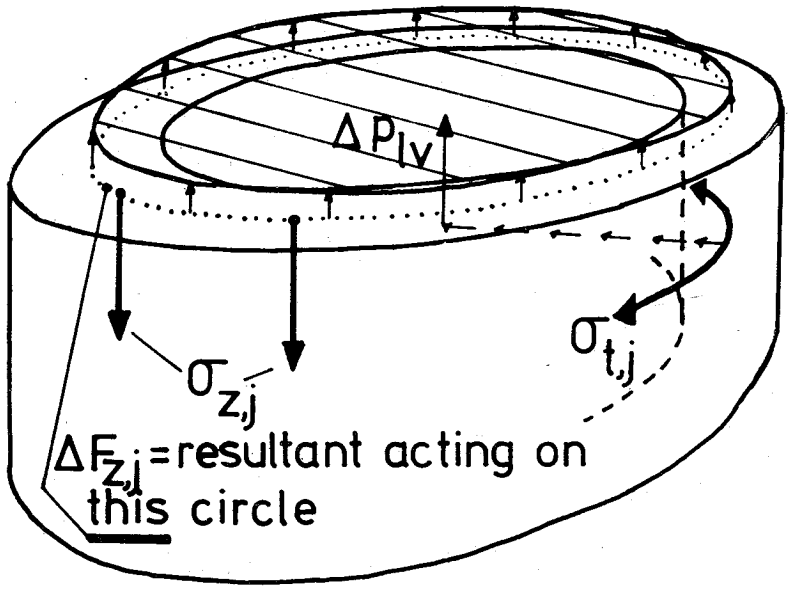

FIGURE 5. Schematic representation of the calculation of the axial force per shell $\Delta F_{z,j}$. According to Laplace's law the tangential stress $\sigma_{t,j}$ generates a pressure Δp_{lv}, which acts on the upper shaded area. The resulting force counteracts the force acting on the upper surface of the wall of the cylinder due to the axial stress $\sigma_{z,j}$.

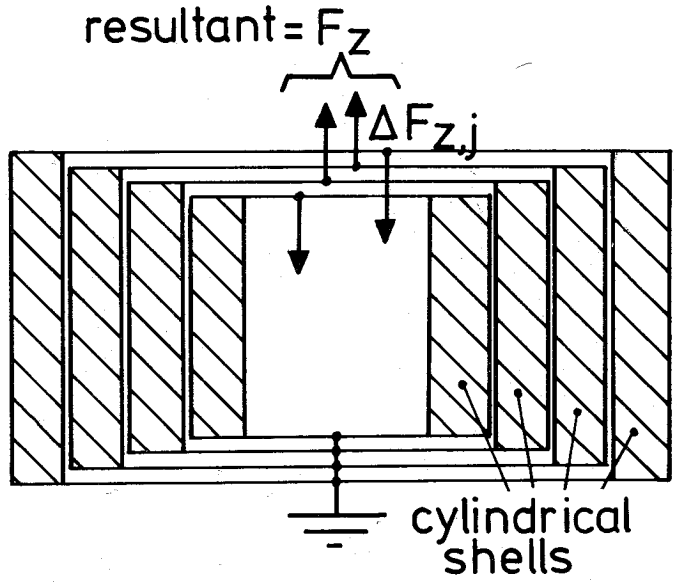

FIGURE 6. In a state of equilibrium the resultant F_z of all forces $\Delta F_{z,j}$ must be zero.

rounded by a thin film of fluid under a hydrostatic pressure, exerted by the surrounding shells.

The axial forces $\Delta F_{z,j}$, necessary to keep the shells in the actual state of deformation, result in the total axial force

$$F_z = \sum_{j=1}^{n} \Delta F_{z,j} \tag{19}$$

The equilibrium of axial forces requires that

$$F_z = 0 \tag{20}$$

In an analogous way the equilibrium of torques in the upper surface is dealt with. Each shell j contributes a torque $\Delta T_{z,j}$ to the total torque T_z acting on the upper surface of the cylinder. The cavity does not contribute. For the torque contribution $\Delta T_{z,j}$ it holds

$$\Delta T_{z,j} = \frac{\pi}{2} (r_{o,j}^2 - r_{i,j}^2)(r_{o,j} + r_{i,j})\, \sigma_{ftz,j} \tag{21}$$

The torque does not depend on hydrostatic pressure. The total torque T_z is described by

$$T_z = \sum_{j=1}^{n} \Delta T_{z,j} \tag{22}$$

The equilibrium of torque in the upper surface requires

$$T_z = 0 \tag{23}$$

The quantities F_z and T_z finally depend on the height h and torsion angle α of the cylinder. Solution of Eqs. 20 and 23 results in the actual values of h and α. In the related calculations a second order iterative procedure is used.

Calculation of Local Intramyocardial Pressures and Left Ventricular Pressure

The intramyocardial pressure is defined as the pressure in the soft material surrounding the myocardial fibers. Since the myocardial fibers are assumed to be parallel to the myocardial wall, the radial component σ_r of the stress in the wall has the opposite value of the local intramyocardial pressure p_{im}.

When applying Laplace's law to the cylinder wall the tangential component of the stress σ_t equals

$$\sigma_t(r) = r \frac{d\sigma_r}{dr} = -r \frac{d\, p_{im}}{dr} \tag{24}$$

When using the model of cylindrical shells, Eq. 24 renders an approximation of the intramyocardial pressure increment $\Delta p_{im,j}$ over one half shell j

$$\Delta p_{im,j} \simeq \sigma_{ft,j} \frac{r_{o,j} - r_{i,j}}{r_{o,j} + r_{i,j}} \tag{25}$$

TABLE 1
Quantities, Describing the Initial State of the Cylinder, Representing the Left Ventricle.

Cavity volume	120.7 ml
Inner radius	22.4 mm
Outer radius	34.4 mm
Height	76.6 mm
Number of shells	8

Fiber Angle in Shells 1 Through 8 (Radians)							
1	2	3	4	5	6	7	8
0.85	0.50	0.30	0.10	−0.05	−0.10	−0.75	−1.45

The value of the intramyocardial pressure $p_{im,j}$ in the central region of shell j is obtained by summation of the intramyocardial pressure increments $\Delta p_{im,j}$, beginning from the outer shell. The external pressure is supposed to be zero. The intramyocardial pressure in the outer shell $p_{im,n}$ is described by

$$p_{im,n} = \Delta p_{im,n} \tag{26}$$

where $\Delta p_{im,n}$ is obtained from Eq. 25. The intramyocardial pressure in each shell is obtained by subsequently applying

$$p_{im,j} = p_{im,j+1} + \Delta p_{im,j+1} + \Delta p_{im,j} \tag{27}$$

starting from $j = n-1$ downwards to $j = 1$. The left ventricular pressure (p_{lv}), which equals the intramyocardial pressure at the endocardial surface, is found as

$$p_{lv} = p_{im,1} + \Delta p_{im,1} \tag{28}$$

SUBSTITUTION OF PARAMETERS IN THE MODEL

As mentioned before the model discussed in this article is part of a larger model describing the dynamic behaviour of cardiac muscle mechanics during contraction. The values of the parameters substituted in the latter model have been described previously (1). Therefore only the value of the parameters relevant to the present study will be discussed.

In analyzing cardiac mechanics, knowledge of initial geometry and fiber orientation is required. In Table 1 the initial, end-diastolic values of height, inner and outer radius of the cylinder, the number of the shells and the fiber angle in each shell are given.

Generally the relation between fiber stress and sarcomere length is characterized by a non-linear passive elastic element parallel to an active element. Thus the active element is characterized by a relation between stress, sarcomere length and velocity of sarcomere shortening which depends on the time varying degree of contraction (1). However, in the present paper a simplification is made by neglecting the influence of velocity of sarcomere shortening

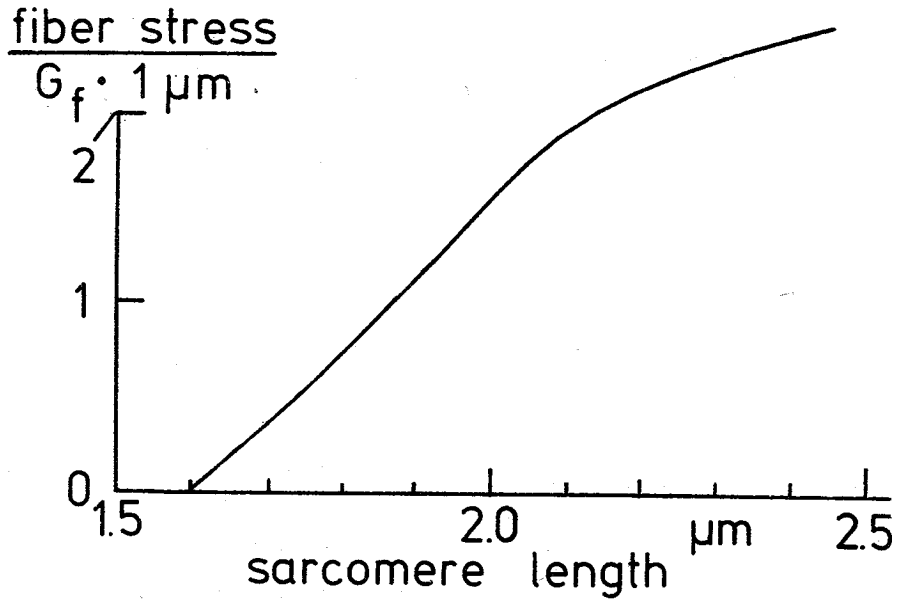

FIGURE 7. Maximum developed fiber stress σ_f as a function of sarcomere length l_s. At l_s = 2.1 μm the fiber stress tends to level off.

on fiber stress, as described elsewhere (21, 27). The relation between fiber-stress (σ_f) and sarcomere length (l_s) is proposed to be

$$\sigma_f = (1 + x - \sqrt{x^2 + 0.01})\, l_s\, G_f \tag{29}$$

with

$$x = \frac{l_s - 2.1\ \mu m}{1\ \mu m}$$

In the following considerations Eq. 29 replaces Eq. 14. Equation 29, represented graphically in Fig. 7, is based on the following experimental results. In experiments on papillary muscle Pollack et al. (19) as well as Sonnenblick et al. (23) reported a proportionality between generated active force and $l_s - 1.6$ μm for sarcomere lengths in the range from 1.6 μm to 2.1 μm. For sarcomere lengths larger than 2.1 μm this force tends to level off (28). At increasing sarcomere length the cross-section of the muscle decreases in such a way that the volume does not change (9). Because of this the fiber stress is proportional to the force multiplied by the sarcomere length. From experiments of Pollack et al. (19) it can be derived that during isosarcometric contraction this proportionality factor (G_f) is equal to $55 \cdot 10^9$ N m^{-3}.

The experiments of Pollack et al. (19) were performed on rat papillary muscles at 26°C. However, the stress developed during an isometric contraction is practically independent of temperature (4, 6). Therefore, Pollack's values are used in the present model.

Suga et al. (27) and Sagawa (21) represent systole by an increase of the Young's modulus of the cardiac material. These investigators concluded a

continuous increase of this Young's modulus during the period of ejection, independent of left ventricular cavity volume. In the present model the factor G_f, which is analogous to the Young's modulus, is assumed to be constant during ejection. The error made by this assumption is an overestimation of stresses and left ventricular pressure of approximately 40% at the beginning of ejection, and decreasing to 0% at the end of ejection. However, this overestimation is uniform across the wall, not affecting the transmural distribution of stress. The relation between left ventricular volume, dimensions and transmural values of sarcomere length is not affected by the assumption G_f is a constant factor.

The sarcomere length at the end of diastole is assumed to be equal to 2.08 μm in all layers. This is based on an average of the findings of Hort (11), Spotnitz et al. (24) and Yoran et al. (30).

RESULTS

For different volumes of the cylinder cavity, representing the left ventricular cavity, the transmural distribution of stress, sarcomere length and intramyocardial pressure as well as left ventricular pressure were calculated during ejection according to the method presented. Since the velocity of sarcomere shortening does not influence fiber stress the described findings also hold for isovolumic contractions. In the present model, left ventricular volume decreases from 120 ml to approximately 60 ml during a normal ejection. How-

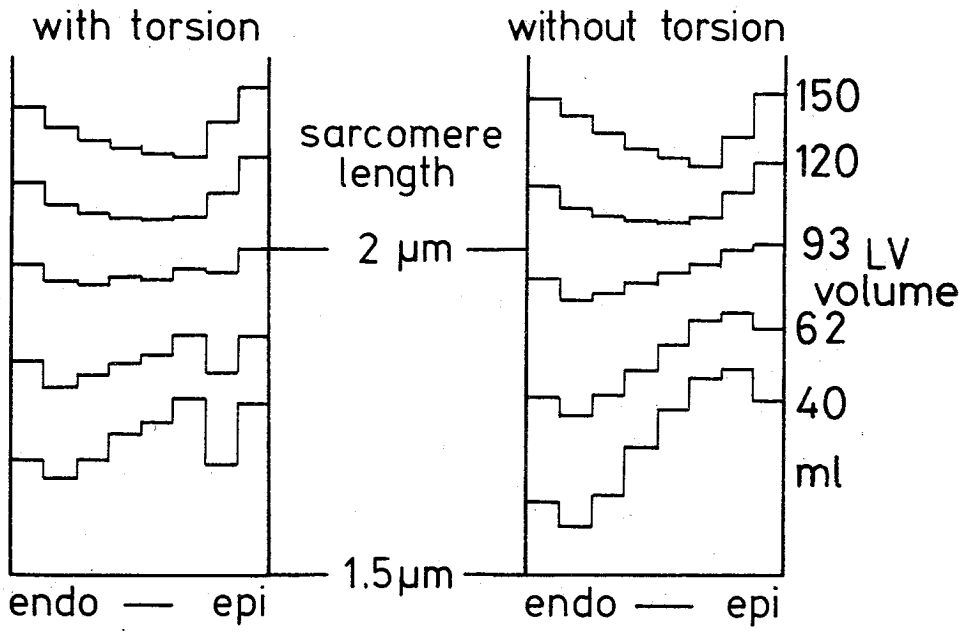

FIGURE 8. Transmural distribution of sarcomere length during systole at different volumes of the cavity of the cylinder as calculated both with and in absence of torsion. During normal ejection LV-volume decreases from 120 to 60 ml in the described model.

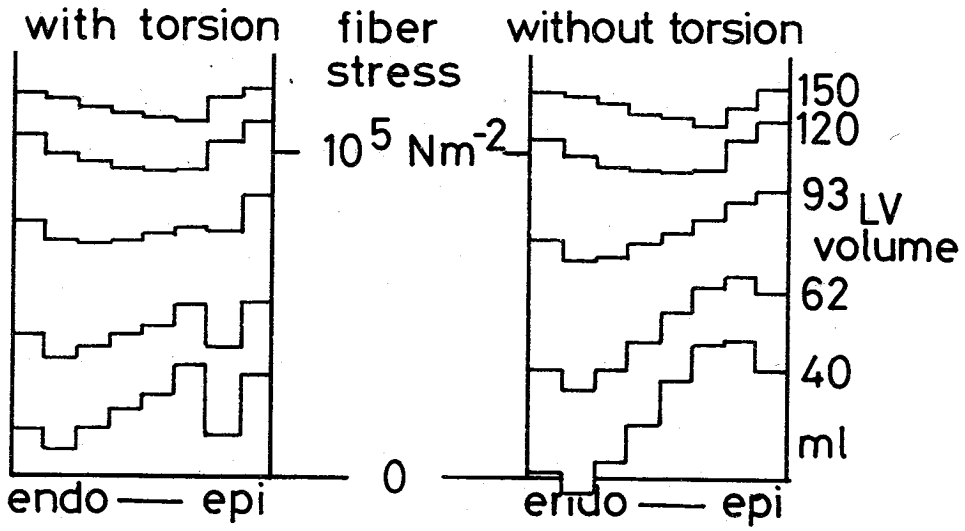

FIGURE 9. Transmural distribution of the fiberstress during systole at different volumes of the cavity of the cylinder both with and in absence of torsion. The conditions are the same as described in Fig. 8.

ever, under various simulated hemodynamic conditions left ventricular volume varied between 40 and 150 ml. The calculations were performed both when considering torsion of the cylinder and when not doing so. The transmural distribution of the sarcomere length at different volumes of the cylinder cavity, in both cases mentioned, are presented in Fig. 8. From these data the transmural distribution of fiber stress, both with and in absence of torsion, is shown in Fig. 9. At the beginning of ejection, all stresses are over-

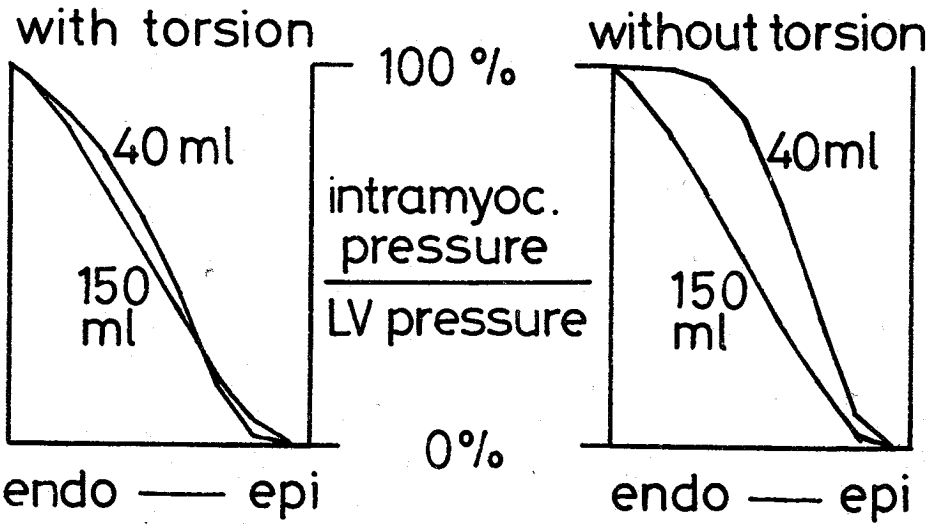

FIGURE 10. Transmural course of the ratio of intramyocardial pressure to left ventricular pressure during systole at different cavity volumes both with and in absence of torsion. The conditions are the same as described in Figure 8.

estimated by approximately 40% as mentioned before. During ejection this overestimation decreases continuously to 0% at the end of ejection. Thus during ejection stress is much more constant in time than would be expected from the data described in Fig. 9. The transmural course of the ratio of intramyocardial pressure to left ventricular pressure at different cavity volumes is presented in Fig. 10. At lower volumes this ratio is large in the subendocardial layers when no torsion is allowed. In Fig. 11 the calculated relation between systolic volume and systolic left ventricular pressure is shown both with and in absence of torsion. From the data presented by Sagawa (21) it can be concluded that the active pressure-volume relation in Fig. 11 is close to the physiological relation as far as the linear increase of pressure with volume at lower volumes and the leveling off of the pressure at the higher volumes are concerned. Moreover, in Fig. 11 the linear extrapolation to low volume levels crosses the zero-pressure level at a low volume (10 ml) as compared to the normal end-diastolic volume, which is also discussed by Sagawa (21). Figure 12 shows the dependence of torsion angle, height, inner and outer radius on cavity volume when torsion occurs. Exclusion of torsion does not affect these dependences, the torsion angle obviously being expected.

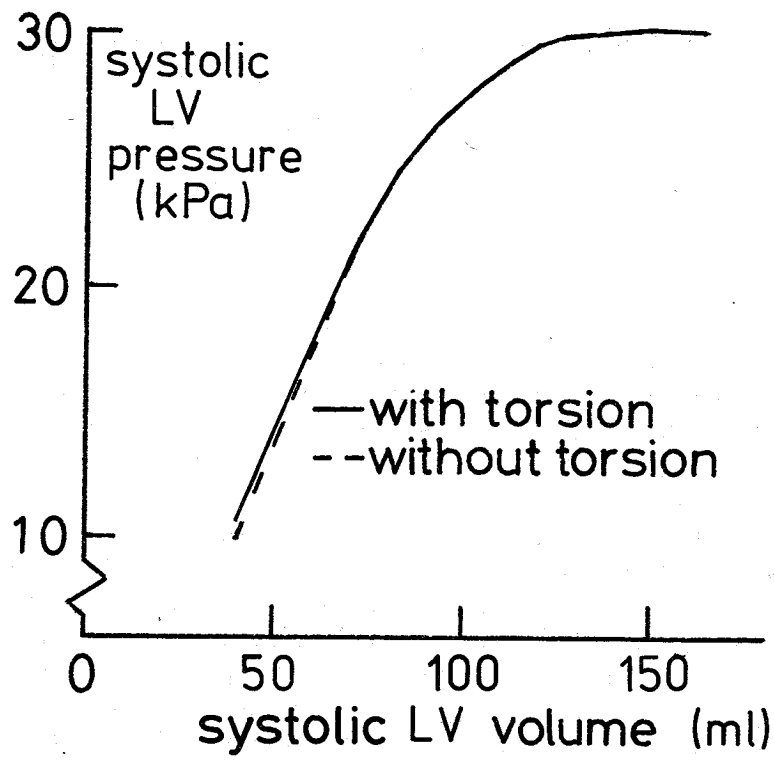

FIGURE 11. Calculated systolic pressure-volume relationship in the left ventricle during isovolumic contraction, both with and in absence of torsion of the left ventricle.

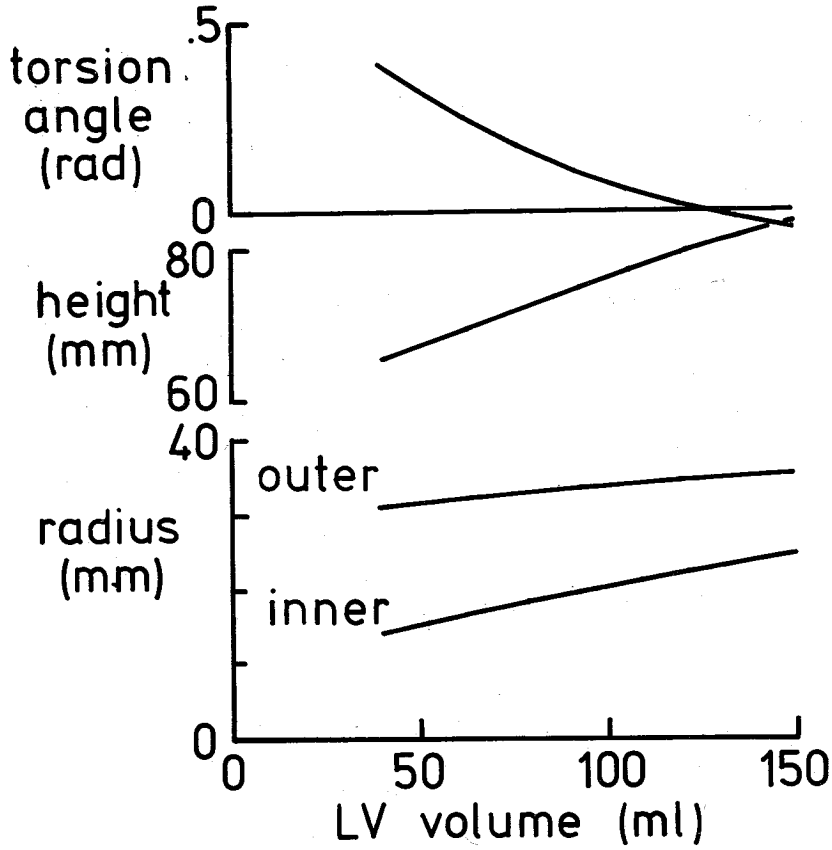

FIGURE 12. Calculated torsion angle, height, inner and outer radius as a function of left ventricular volume during systole when torsion is allowed.

DISCUSSION

The present model reveals that, when torsion is admitted, the transmural course of sarcomere length and tensile muscle stress is rather uniform at various filling volumes (Figs. 8 and 9). The findings suggest a rather uniform distribution of all quantities relevant for cardiac muscle mechanics and, probably, to cardiac energetics. This result is essentially different from the results of studies on ventricular mechanics as performed by Wong et al. (29) and Hood et al. (10). They found that during systole subendocardial stress was approximately twice as high as subepicardial stress. This discrepancy can be explained by the fact that these authors assumed isotropy of the cardiac muscle material, as distinct from the present assumption of anisotropy. This explanation is supported by the finding in the model that at a value of left ventricular pressure during isovolumic contraction of 30 kPa induced by cross-clamping the aorta, muscle stress did not exceed 125.10^3 N m^{-2} (= 12.5 gr.mm^{-2}) at a sarcomere length of 2.2 μm, which is in agreement with experiments on the force length relation in isolated cardiac muscle (19). In

models based on isotropy of cardiac muscle, similar left ventricular pressure values can often only be obtained by introducing an active stress, which is approximately three times higher than in the present model (8).

The uniformity of the transmural distribution of stress and sarcomere length can be explained by the nature of the transmural course of the fiber orientation. The transmural course of tensile muscle stress is mainly determined by forces and torques in the upper surface of the cylinder. Layers with a fiber angle close to 45° and those with that angle close to −45° counterbalance through the equilibrium of torques in the upper surface of the cylinder. Layers with mainly axially and tangentially directed fibers counterbalance in the upper surface of the cylinder through the equilibrium of axial forces. Considering the real ventricle, this might mean that the layers between the center and subepicardium counterbalance with the subendocardial layers through the equilibrium of torques, whereas the center layers counterbalance the subepicardial layers through the equilibrium of axial forces. The transmural course of the fiber orientation determines the thickness of the layers, which are involved in these equilibria and, thus, determines the transmural distribution of tensile muscle stress. Despite the fact that the torsion angle of the cylinder varies considerably at different cavity volumes, the transmural course of the fiber angle is approximately constant, thus maintaining a uniform distribution of fiber stress at different filling volumes. Disturbing the equilibrium of torques in the upper surface by preventing torsion makes the transmural distribution of stress and sarcomere length less uniform. This non-uniformity is most pronounced at low filling volumes (Figs. 8 and 9) because subendocardial deformation is largest under those circumstances. The non-uniformity does not considerably affect the pressure volume relationship (Fig. 11).

When the volume of the left ventricular cavity decreases, circumferential shortening is more pronounced in the subendocardial than in the subepicardial layers. However, fiber shortening appears to be nearly the same in these layers. This paradox can be explained by torsion of the cylinder, thus equalyzing the amount of shortening of the subendocardial and subepicardial fibers. This is made possible by the presence of an appropriate transmural course of fiber orientation. If torsion is prevented, transmural differences in sarcomere shortening are more pronounced (Fig. 8).

Except for its magnitude, the transmural course of intramyocardial pressure is rather similar under various conditions, because transmural differences in tensile muscle stress are small at various cavity volumes. Because of boundary conditions intramyocardial pressure equals left ventricular pressure at the endocardium and equals zero at the epicardium. Thus in all layers of the myocardium, intramyocardial pressure is approximately proportional to left ventricular pressure. At the endocardium the related proportionality factor equals unity, whereas at the epicardium this factor equals zero (Fig. 10). If torsion is prevented, this proportionality factor depends more strongly on left ventricular volumes.

The validity of the part of the model described in this paper is demonstrated by the fair agreement between the results obtained in the extensive model and obtained in animal experiments at least as far as left ventricular pressure, aortic pressure and volume flow and left ventricular dimensions are concerned. Animal experiments for instance, showed that the base to apex distance increased during the isovolumic contraction phase by 2.1% and decreased during the ejection phase by 6.2% (20). The inner minor axis of the left ventricle decreased during systole by 22% in these experiments. In the present model the changes in these variables were found to be 2.3%, 6.3% and 23%, respectively. Although it is beyond the scope of this article to discuss in detail animal experiments, an additional comparison between the results obtained in the model and in a dog experiment is presented in Fig. 13. In the right panel the time courses of left ventricular pressure, aortic pressure and aortic volume flow, as well as axial and circumferential strain of the outer surface, as generated by the model, are shown. In this simulation corrections were made for unequal time of onset of contraction and the influence of velocity of sarcomere shortening on the generation of active stress (1). During ejection, especially in the second part of this phase of the cardiac cycle, these corrections are of minor importance, allowing application of the simplified model as presented in this paper. In the left panel the same quantities are shown, as obtained in the intact dog. Left ventricular and aortic pressures were measured with Millar cathether tip micromanometers. Aortic volume flow was determined electromagnetically. Axial and circumferential strain were calculated from the segment lengths, as measured from base to

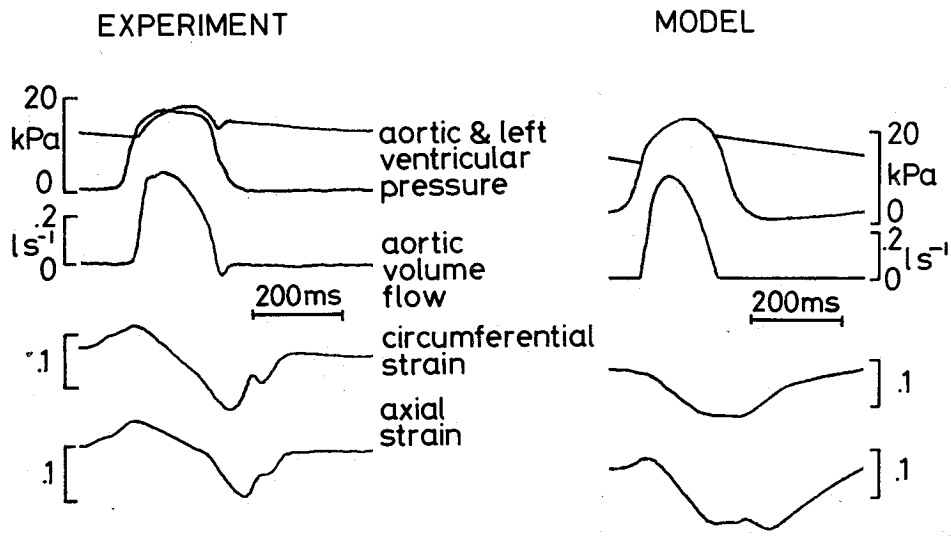

FIGURE 13. Comparison of the results as obtained in the mathematical model (right panel) and in dog experiments (left panel), as far as cardiac hemodynamics and epicardial strains are concerned.

apex and along the circumference on the anterior part of the left ventricular free wall. From Fig. 13 it can be concluded that the results as obtained in the model and the animal experiment are qualitatively and quantitatively in good agreement at least within the limits of biological variance.

In conclusion, torsion of the apex with respect to the base around the axis of the left ventricle may play an important role in equalizing differences in mechanical work across the left ventricular wall. The present model is an effective tool in describing quantitatively the mechanics of the wall of the left ventricle and, more generally, in understanding the mechanism of left ventricular contraction.

REFERENCES

1. Arts, M. G. J. A mathematical model of the dynamics of the left ventricle and the coronary circulation. Thesis, University of Limburg, The Netherlands, 1978.
2. Arts, T., and R. S. Reneman. Analysis of intramyocardial pressure (IMP). A model study. *Bibl. Anat.* 15:103–107, 1977.
3. Back, L. Left ventricular wall and fluid dynamics of cardiac contraction. *Math. Biosci.* 36:257–297, 1977.
4. Binkhorst, R. A., L. Hoofd, and A. C. A. Vissers. Temperature and force-velocity relationship of human muscles. *J. Appl. Physiol.* 42:471–475, 1977.
5. Durrer, D., R. Th. van Dam, G. E. Freud, M. J. Janse, F. L. Meyler, and R. C. Arzbaecher. Total excitation of the isolated human heart. *Circulation* 41:899–912, 1970.
6. Edman, K. A. P. and E. Nilsson. The mechanical parameters of myocardial contraction studied at a constant length of the contractile element. *Acta Physiol. Scand.* 27:205–219, 1968.
7. Gould, P., D. Ghista, and L. Brombolich. In vivo stresses in the human left ventricular wall: Analysis accounting for the irregular 3-dimensional geometry and comparison with idealised geometry analyses. *J. Biomech.* 5:521–539, 1972.
8. Hanna, W. T. A simulation of human heart function. *Biophys. J.* 13:603–621, 1973.
9. Hill, A. V. A discussion on muscular contraction and relaxation: Their physical and chemical basis. Proc. R. Soc. London, Ser. B 137:40–87, 1950.
10. Hood, W. P. Jr., W. J. Thomson, C. E. Rackley, and E. L. Rolett. Comparison of calculations of left ventricular wall stress in man from thin-walled and thick-walled ellipsoidal models. *Circ. Res.* 24:575–582, 1969.
11. Hort, W. Makroskopische und mikrometrische Untersuchungen am Myocard verschieden stark gefüllter linker Kammern. *Virchows Arch. Pathol. Anat.* 333:523–564, 1960.
12. Janz, R. F. and A. F. Grimm. Finite-element model for the mathematical behaviour of the left ventricle. *Circ. Res.* 30:224–252, 1972.
13. Janz, R. F. and A. F. Grimm. Deformation of the diastolic left ventricles: I. Non-linear elastic effects. *Biophys. J.* 13:589–704, 1973.
14. McHale, P. A. and J. C. Greenfield. Evaluation of several geometric models for estimation of left ventricular circumferential wall stress. *Circ. Res.* 33:303–312, 1973.
15. Mirsky, I. Left ventricular stresses in the intact human heart. *Biophys. J.* 9:189–208, 1969.
16. Mirsky, I. Ventricular and arterial wall stresses based on large deformation analysis. *Biophys. J.* 13:1141–1159, 1973.
17. Pao, Y. C., E. L. Ritman, and E. H. Wood. Finite element analysis of left ventricular myocardial stresses. *J. Biomech.* 7:469–477, 1974.
18. Pao, Y. C., R. A. Robb, and E. L. Ritman. Plain-strain finite-element analysis of reconstructed diastolic left ventricular cross-section. *Ann. Biomed. Eng.* 4:232–249, 1976.
19. Pollack, G. H. and J. W. Krueger. Sarcomere dynamics in intact cardiac muscle. *Eur. J. Cardiol.* 4:53–65, 1976.
20. Rankin, J. S., P. McHale, C. E. Arentzen, D. Ling, J. C. Greenfield, and R. W. Anderzon. The three-dimensional dynamic geometry of the left ventricle in the conscious dog. *Circ. Res.* 39:304–313, 1976.
21. Sagawa, K. The ventricular pressure-volume diagram revisited. *Circ. Res.* 43:677–687, 1978.

22. Scher, A. M. and A. C. Young. The pathway of ventricular depolarisation in the dog. *Circ. Res.* 4:461–469, 1956.
23. Sonnenblick, E. H., D. Spiro, and T. S. Cottrell. Fine structural changes in heart muscle in relation to the length tension curve. *Proc. Nat. Acad. Sci. USA.* 49:193–200, 1963.
24. Spotnitz, H. M., E. H. Sonnenblick, and D. Spiro. Relation of ultrastructure to function in intact heart. Sarcomere structure relative to pressure-volume curves of intact left ventricles of dog and cat. *Circ. Res.* 18:49–66, 1966.
25. Streeter, D. D., H. M. Spotnitz, D. P. Patel, J. Ross, and E. H. Sonnenblick. Fiberorientation in the canine left ventricle during diastole and systole. *Circ. Res.* 33:656–664, 1973.
26. Streeter, D. D., R. N. Vaishnav, D. J. Patel, H. M. Spotnitz, J. Ross, and E. H. Sonnenblick. Stress distribution in the canine left ventricle during diastole and systole. *Biophys. J.* 10:345–363, 1970.
27. Suga, H. and K. Yamakoski. Left ventricle as a compression pump. *Eur. J. Cardiol.* 4:97–103, 1976.
28. Ter Keurs, H. E. D. J., T. Iwazumi, and G. H. Pollack. Sarcomere length-tension relation in skeletal muscle. *J. Gen. Physiol.* 27:565–592, 1978.
29. Wong, A. Y. K. and P. M. Rautoharju. Stress distribution within the left ventricular wall approximated as a thick ellipsoidal shell. *Am. Heart J.* 75:649–661, 1968.
30. Yoran, C., J. W. Covell, and J. Ross. Structural basis for the ascending limb of left ventricular function. *Circ. Res.* 32:297–303, 1973.